Investigation of Carbohydrate Metabolism and Transport in Castor Bean Seedlings by Cyclic *J* Cross Polarization Imaging and Spectroscopy

M. Heidenreich,*,1 W. Köckenberger,† R. Kimmich,* N. Chandrakumar,*,2 and R. Bowtell†

Sektion Kernresonanzspektroskopie, Universität Ulm, 89069 Ulm, Germany; and †Magnetic Resonance Centre, Department of Physics, University of Nottingham, Nottingham NG7 2RD, United Kingdom

NMR experiments using ^{13}C-labeled compounds offer the possibility of noninvasive monitoring of carbohydrate transport and metabolism in living plants, but are usually hampered by the low sensitivity of the ^{13}C nucleus. The problem of low sensitivity can be overcome by using the cyclic *J* cross polarization (CYCLCROP) technique, which allows the indirect detection of ^{13}C nuclei coupled to ^{1}H nuclei with the high NMR sensitivity of protons. We report here on methods for imaging and spectroscopy based on the CYCLCROP technique, and their use in the first *in vivo* NMR study of carbohydrate transport and metabolism in castor bean seedlings (*Ricinus communis L.*). Comprehensive acquisition strategies for the various NMR methods are given, including the procedure for setting up the experiments. In addition, a full analysis of the effect of relaxation on the signals generated from small *J*-coupled spin systems by the CYCLCROP sequence is given, and the high sensitivity of the sequence is demonstrated. In the *in vivo* study of six-day-old castor bean seedlings, we were able to measure the uptake of labeled hexoses, supplied in solution to the cotyledons, and their conversion to sucrose, as well as the transport of this sucrose in the vascular bundles. Images of the actual distribution of labeled sucrose in the hypocotyl of the seedling have also been obtained. The resulting data show some evidence for a preferential incorporation of labeled fructose in the process of sucrose synthesis, which decreases with the time of incubation. © 1998 Academic Press

Key Words: cyclic cross polarization; indirect ^{13}C NMR imaging; sucrose metabolism; transport in plants.

INTRODUCTION

The products of photosynthesis and CO_2 assimilation in plants are energy-rich compounds (mainly carbohydrates), which must be transported over long distances from the site of their synthesis (source) to their consumption sites (sinks) such as growing tissues, storage organs, and roots. The major transport form of carbohydrates in plants is the disaccharide sucrose. Plants possess within their vascular bundles special-ized cells, the sieve tubes of the phloem, in which the transport takes place. Compounds such as sucrose or amino acids are loaded by carriers into the sieve tubes within the source organs, thus creating a difference in osmotic pressure across the semi-permeable membrane. Water enters the sieve tubes through the membrane because of the difference in osmotic pressure. Within the sink region compounds are unloaded from the sieve tubes, and water simultaneously exits the phloem pathway, a process which leads to differences in hydrostatic pressure between the sources and the sinks. The pressure gradient creates a water flow within the sieve tubes and the compounds of the phloem sap are carried passively from sources to sinks.

Since sieve tubes are embedded in parenchymatic tissue, the direct determination of their contents is difficult and consequently a quantitative characterization of transport is a demanding problem. Indirect techniques such as labeling of the transported compounds by radioactive tracers, such as ^{14}C or ^{11}C, or injection of dyes, which are transported within the phloem, have previously been used to characterize transport. After the application of ^{14}C, plants must be harvested to allow measurement of the accumulated radioactivity in the different parts. One disadvantage of this technique is that it is destructive and therefore does not allow repetitive measurements to be performed on one plant. Such repeated measurements are valuable since they allow the investigation of changes in transport as a response to alterations in the environment of the plant. Transport of the tracer ^{11}C between different parts of an intact plant can be observed by an appropriate positioning of monitors, and therefore this technique is nondestructive. However, since ^{11}C is supplied to plants as [11]CO_2, the chemical nature of the compound which carries the label after assimilation cannot easily be identified. Movement of dyes in the sieve tubes indicates water flow in the phloem, but represents only an indirect estimation of solute transport.

Recently it has been demonstrated that MRI techniques are versatile tools for studying transport processes in plants. These techniques are noninvasive, and in addition they allow

the spatially resolved measurement of a variety of physical and chemical parameters within the plant. Pulsed gradient spin-echo techniques have been used to measure the velocity of water flow in xylem vessels (*1, 2*) or in both xylem vessels and phloem sieve tubes of intact plants (*3*). A chemical shift imaging technique has also been used to quantify the concentration of sucrose in the intact phloem of castor bean seedlings (*4*).

NMR experiments using ^{13}C-labeled compounds offer the possibility of noninvasive monitoring of carbohydrate transport, but are usually hampered by the low sensitivity of the ^{13}C nucleus (*5*). We report here on experiments in which we used indirect ^{13}C detection by *cycl*ic *J cro*ss *p*olarization (CYCLCROP) (*6–8*) to overcome the sensitivity problem, thus allowing studies of the transport and metabolism of sucrose in plants *in vivo*. The experimental protocol offers several advantages. (i) Noninvasive measurements of the undisturbed situation in the intact plants can be performed. (ii) The transported compound is unambiguously identified by its characteristic resonance lines. (iii) Transport can be studied by observing changes of the signal intensity of ^{1}H nuclei coupled to ^{13}C. (iv) Spatially resolved information about the distribution of the compound within the plant can be obtained by combining CYCLCROP with imaging techniques.

We carried out the experiments with six-day-old castor bean seedlings because (i) seedlings have been used extensively as a model system for the investigation of phloem transport, both with standard (*9*) and with NMR techniques (*3, 4, 10*). Consequently a large amount of information on the physiology of the seedlings is readily available. (ii) The cotyledons take up sugars from the incubation medium, and therefore labeled compounds can easily be introduced into the plant without affecting the natural concentration of the compound within the plant. (iii) The small size and the independence of the seedlings from lighting mean that they can easily be grown in the bore of a superconducting magnet.

THEORETICAL BACKGROUND

The CYCLCROP Editing Sequence

The basic pulse sequence for indirect detected ^{13}C imaging by cyclic cross polarization consists of two parts, the editing part and the imaging part (Fig. 1) (*8*). The editing part of the sequence serves to select a single resonance from a specific site of a molecule while suppressing all other resonances from the sample. The imaging part provides spatially resolved information about the density of the selected molecular species within the sample. In conventional proton NMR imaging, contrast is mainly created by the spatial dependence of relaxation parameters. In contrast, in the CYCLCROP imaging experiment one is interested in minimizing the effects of relaxation to obtain maps of the spin density of a molecular species.

In order to understand the principle of the editing sequence, let us consider a small spin system $I_N S$ of *J*-coupled spins *I* and *S*, such as the CH_2 group of a sucrose molecule in solution, for example. Here, *S* spins correspond to the ^{13}C nuclei, *I* spins to protons. In the first step, the Zeeman polarization of the low sensitivity nuclei *S* is maximized by an initial polarization transfer from the directly coupled *I* spins to the *S* spins. This *S* magnetization is subsequently stored along the *z* direction. A number of consecutive pulses at the resonance frequency of the *I* spins in combination with spoiler gradient pulses ensures complete saturation of all residual *I* spin resonances. Thereafter, the second polarization transfer from *S* spins to the directly coupled *I* spins of the $I_N S$ system brings back the coherence to the *I* spins, where it can be used further for imaging or spectroscopic applications. The only contribution to the detected signal comes from *I* spins which are coupled to the *S* spins within the selected molecular group. This process of two consecutive polarization transfers between the *I* and *S* spins combines the high spectral selectivity of the *S* spins with the maximum NMR sensitivity given by detection of the *I* spins.

Two major advantages make polarization transfer techniques operating in the rotating frame (as compared with techniques employing polarization transfer in the laboratory frame, like INEPT (*11*)) particularly appropriate for *in vivo* applications: (i) They result in a direct production of in-phase coherences, and (ii) they are relatively insensitive to sample movements during the measurement (*7*). Polarization transfer between two nuclei *I* and *S* in the rotating frame can be achieved by a number of techniques. The basic technique, *J* cross polarization (JCP), was originally proposed by Hartmann and Hahn in 1962 (*12*). The transfer starts with an excitation pulse followed by a spin lock pulse (SL) on the primary side (nuclei *I*) and a contact pulse (CP) applied on the secondary side (nuclei *S*). Polarization transfer takes place if SL and CP are matched according to the Hartmann/Hahn condition

$$\gamma_I B_{1,\text{eff},I} = \gamma_S B_{1,\text{eff},S}, \qquad [1]$$

where γ_I and γ_S are the gyromagnetic ratios of the nuclei under consideration and $B_{1,\text{eff},I}$ and $B_{1,\text{eff},S}$ are the magnetic flux densities effective in the doubly rotating frame.

The duration of the optimum contact time depends on the size of the spin system, the *J* coupling constant, possible Hartmann/Hahn mismatch conditions with respect to RF amplitudes and/or deviations from resonant irradiation, and relaxation effects as will be pointed out in the following section. The disadvantage of the basic JCP technique is its small tolerance of Hartmann/Hahn mismatch which is on the order of the *J* coupling constant, with typical values of 120 to 170 Hz for ^{1}H–^{13}C spin pairs. However, this disadvantage can be overcome by using the MOIST modification (*13, 14*) of polarization transfer. In this variant, the
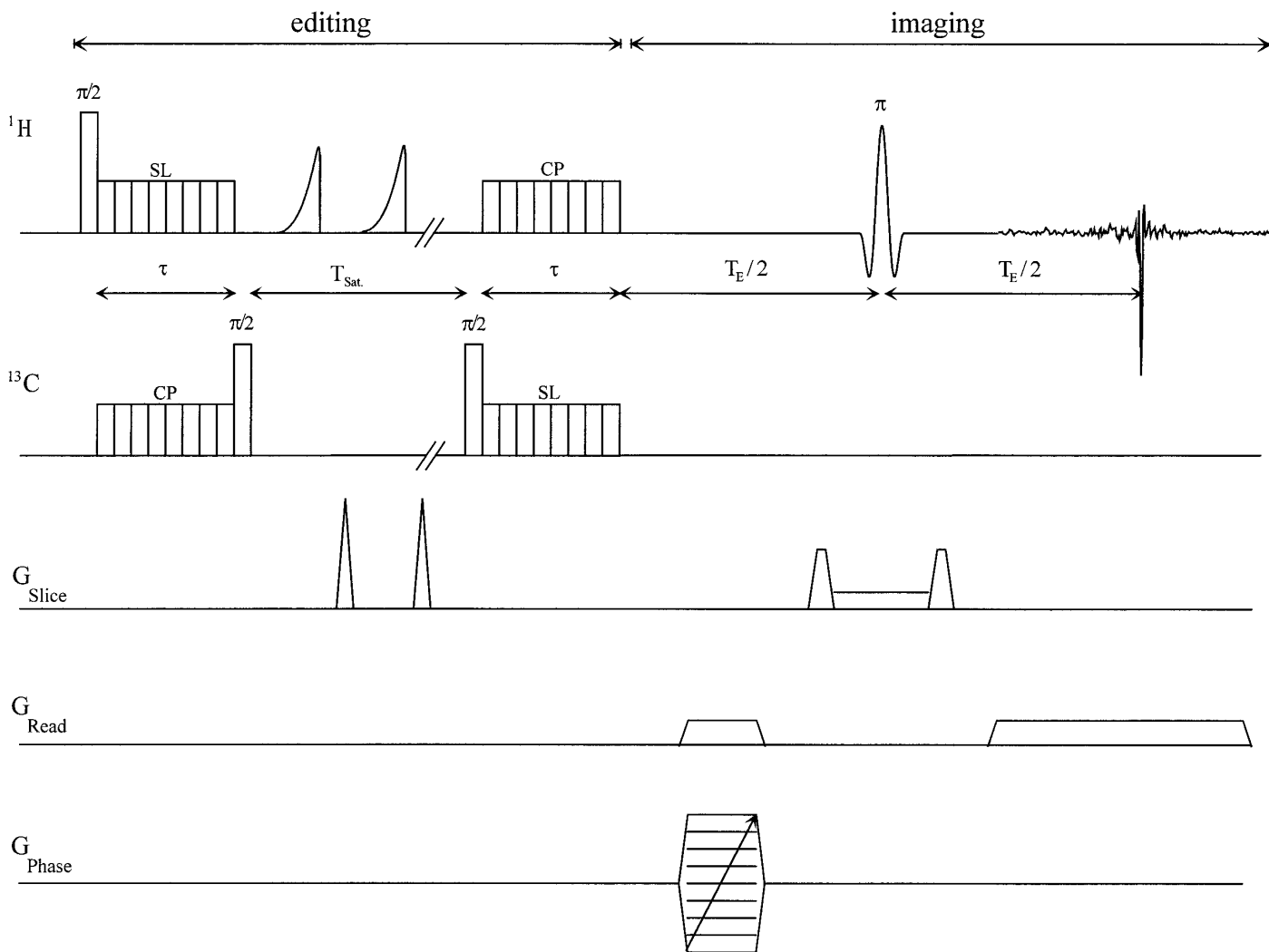
FIG. 1. Radiofrequency and field gradient pulse sequence for the CYCLCROP imaging technique yielding indirect ^{13}C images via proton signals. The first part of the sequence serves the editing of resonance lines of protons (I spins) coupled to ^{13}C nuclei (S spins). The principle of the technique is cyclic polarization transfer in the rotating frame which is performed in a forward, $I \to S$, and a backward step, $S \to I$. In each of these steps, a spin-locking pulse (SL) on the primary side and a contact pulse (CP) on the secondary side are applied and matched according to the Hartmann/Hahn condition. For ease of adjustment, the MOIST modification of the Hartmann/Hahn sequence is employed. During SL and CP pulses, the phases are inverted simultaneously. For maximal signal strength, the JCP is optimized according to the NMR properties of the hydrocarbon group of interest (chemical shifts, J couplings, and size of the spin system) as described in the text. After the first polarization transfer, the selected coherence is stored along the z axis, and a comb of adiabatic half passages, each followed by spoiling gradients, is used to saturate all I spin coherences. The second part of the sequence with slice selection (G_{Slice}), read (G_{Read}), and phase encoding (G_{Phase}) gradients produces spin echo NMR images of the distribution of protons which are coupled to ^{13}C nuclei in the selected hydrocarbon group.

SL and CP pulses are divided into consecutive segments which have π-shifted phases. Under ideal Hartmann/Hahn conditions, the contact times are the same as those for the original JCP sequence. However, the mismatch behavior of the MOIST sequence is determined by the number of phase inversions and the applied B_1 field strengths during SL and CP. Both these parameters are under the control of the experimenter.

Signal Strength of Indirect S Spin Detection

In the following section we treat the general case of cyclic polarization transfer within a J-coupled spin system con-sisting of nuclei I and S. In order to establish a relation between the detectable signal strength and the S spin density distribution, we will examine the evolution of the density matrix during the editing part of this sequence for the most common spin systems in this context (IS, I_2S and I_3S). For the sake of simplicity, we assume in all cases ideal Hartmann/Hahn matching. The influence of Hartmann/Hahn mismatch on the evolution of the density matrix for the single polarization transfer has been treated elsewhere (*15, 16*) and is straightforward enough to apply to the cyclic case.

Assuming presaturation of the S spins (which can be

achieved either by S spin saturation pulses or indirectly by the use of an appropriate phase cycling scheme), the reduced density matrix after the first excitation pulse $((\pi/2)_y(I))$ can be written as

$$\sigma^i_{I_N S} = \sum_{k=1}^{N} I_{x,k} \quad N = \begin{cases} 1 & \text{for the } IS \text{ system} \\ 2 & \text{for the } I_2 S \text{ system} \\ 3 & \text{for the } I_3 S \text{ system,} \end{cases} \quad [2]$$

where the spin operators of the nuclei I and S are denoted by $\mathbf{S} = (S_x, S_y, S_z)$ and $\mathbf{I} = (I_x, I_y, I_z)$, respectively. The influence of the effective Hamiltonian $\hat{H}_{\text{eff}}$ in the doubly rotating frame caused by the simultaneous application of RF fields along the x axis can be calculated by using the Liouville/von Neumann equation. This yields a time-dependent polarization transfer from I to S spins driven by

$$\hat{H}_{\text{eff}} = \frac{J}{2} \sum_{i=1}^{N} (I_{z,i} S_z + I_{y,i} S_y). \quad [3]$$

We thus find for the IS system

$$\sigma_{IS} = \frac{1}{2} I_x(1 + c_J) + \frac{1}{2} S_x(1 - c_J) + (I_y S_z - I_z S_y)s_J,$$
$$[4]$$

for the $I_2 S$ system

$$\sigma_{I_2 S} = \frac{1}{4} (I_{x,1} + I_{x,2}) (3 + c_{\sqrt{2}J}) + \frac{1}{2} S_x(1 - c_{\sqrt{2}J})$$
$$+ (I_{z,1} I_{z,2} + I_{y,1} I_{y,2}) S_x(1 - c_{\sqrt{2}J})$$
$$+ \frac{1}{\sqrt{2}} ((I_{y,1} + I_{y,2}) S_z - (I_{z,1} + I_{z,2}) S_y)s_{\sqrt{2}J}, \quad [5]$$

and for the $I_3 S$ system

$$\sigma_{I_3 S} = (I_{x,1} + I_{x,2} + I_{x,3}) \left(\frac{19}{24} + \frac{1}{12} \left(c_J + c_{\sqrt{3}J} + \frac{1}{2} c_{2J} \right) \right)$$
$$+ S_x \left(\frac{5}{8} - \frac{1}{4} \left(c_J + c_{\sqrt{3}J} + \frac{1}{2} c_{2J} \right) \right)$$
$$+ \frac{1}{3} S_x (I_{y,1} I_{y,2} + I_{y,2} I_{y,3} + I_{y,1} I_{y,3} + I_{z,1} I_{z,2}$$
$$+ I_{z,2} I_{z,3} + I_{z,1} I_{z,3}) (1 + c_J - c_{\sqrt{3}J} - c_{2J})$$
$$+ \frac{1}{6} ((I_{y,1} + I_{y,2} + I_{y,3}) S_z$$
$$- (I_{z,1} + I_{z,2} + I_{z,3}) S_y) (s_J + \sqrt{3}s_{\sqrt{3}J} + s_{2J})$$
$$+ (I_{z,1} I_{z,2} I_{z,3} S_y - I_{y,1} I_{y,2} I_{y,3} S_z) (2s_J - s_{2J}) \quad [6]$$

with $s_{kJ} = \sin(k\pi J\tau)$ and $c_{kJ} = \cos(k\pi J\tau)$. For the $I_3 S$ system, only the relevant terms have been taken into account. A complete treatment of all terms can be found in (17–19).

Equations [4], [5], and [6] describe the time dependences of the density matrices $\sigma_{I_N S}(\tau)$ for the single polarization transfer $I \to S$. Note that only for the IS system is the complete initial I spin polarization transfered to the S spins. For larger spin systems, only a partial polarization transfer is possible, in conformity with bounds on unitary evolution (20, 21). For the $I_2 S$ system the efficiency of the JCP experiment reaches this upper bound while the transfer in the $I_3 S$ system is below. During saturation of the I spins, the S polarization is stored along the z axis and is therefore unaffected by I spin radiofrequency pulses or spoiler gradient pulses. The saturation of all coherences represented by I spin operators will result in an initial state of the density matrix for the back-transfer $S \to I$ which contains only pure in-phase S_x coherences. To calculate the time dependence of the final state of the density matrix, it is useful to apply the commutation relation

$$[\hat{H}_{\text{eff}}, \sum_{k=1}^{N} (I_{x,k}) + S_x] = 0 \quad \text{for} \quad N = 1, 2, 3. \quad [7]$$

This leads to the final density matrix containing the same operators as described in Eqs. [4], [5], and [6]. If a readout gradient is applied during acquisition or if the signal is decoupled or a $\pi/2$ termination pulse is applied to the S spins at the end of the contact period, antiphase I coherences do not contribute to the final density matrix representing the coherences to be observed, and therefore it can be written as

$$IS: \sigma^f_{IS}(2\tau) = \frac{1}{4} (1 - c_J)^2 \sigma^i_{IS} \quad [8]$$

$$I_2 S: \sigma^f_{I_2 S}(2\tau) = \frac{1}{8} (1 - c_{\sqrt{2}J})^2 \sigma^i_{I_2 S} \quad [9]$$

$$I_3 S: \sigma^f_{I_3 S}(2\tau) = \left(\frac{5}{24} - \frac{1}{12} \left(c_J + c_{\sqrt{3}J} + \frac{1}{2} c_{2J} \right) \right)$$
$$\times \left(\frac{5}{8} - \frac{1}{4} \left(c_J + c_{\sqrt{3}J} + \frac{1}{2} c_{2J} \right) \right) \sigma^i_{I_3 S}$$
$$[10]$$

Neglecting relaxation effects for the moment, the optimum contact times τ_0 for the cyclic polarization transfer can be derived as

$$\tau_0 = \begin{cases} J^{-1} & \text{for the } IS \text{ system} \\ (\sqrt{2}J)^{-1} & \text{for the } I_2 S \text{ system} \\ \approx 0.61 J^{-1} & \text{for the } I_3 S \text{ system.} \end{cases} \quad [11]$$

Finally, the time-dependent coefficients of Eqs. [8] to [10] can be evaluated by using the contact times τ_0 in Eq. [11]:

$$IS: \sigma_{IS}^f = \sigma_{IS}^i \qquad [12]$$

$$I_2S: \sigma_{I_2S}^f = 0.5\, \sigma_{I_2S}^i \qquad [13]$$

$$I_3S: \sigma_{I_3S}^f \approx 0.37\, \sigma_{I_3S}^i. \qquad [14]$$

From Eqs. [12], [13], and [14], the I spin magnetization M and therefore the signal strength can be calculated with $M_x \propto \mathrm{Tr}[\sigma_{I_NS}^f I_x]$. Note that for the IS and the I_2S spin systems, the detected I spin signal strength depends entirely on the spin density of the low sensitivity S nuclei. The signal arising from I_3S spin systems is only 11% higher than the signals arising from the IS or I_2S spin system. Therefore, in contrast to conventional proton spectroscopy or spectroscopic imaging, the observed proton signal in the CYCLCROP experiment is almost independent of the size of the spin system under consideration. Rather, it depends on the actual (spin S) density of the coupling partners, giving the same dependence as if the S spin were detected directly (this justifies the term *indirect ^{13}C imaging*). The maximal signal enhancement for all different spin systems which can be achieved using the CYCLCROP experiment is given by a factor of $(\gamma_I/\gamma_s)^3$, compared to single-pulse S spin detection with I spin decoupling and without taking any effects of possible NOE enhancement or noise into account (for the ^{1}H–^{13}C spin pair, this factor would be ≈ 64). However, relaxation processes have a strong influence during the sequence, and therefore the actual signal enhancement which is produced by the cyclic polarization transfer can be considerably smaller than this theoretical factor.

Effects of Relaxation on the Signal Strength

In order to evaluate the effects of relaxation, it is instructive to consider in the following section the particular nuclei under investigation in this study, protons which are scalar coupled to ^{13}C nuclei. If the experiment is repeated, longitudinal proton relaxation processes limit the achievable increase in signal-to-noise ratio by restricting the number of repetitions for a given time interval. Since T_1 relaxation times of ^{1}H nuclei are in general considerably shorter than those of ^{13}C nuclei, the CYCLCROP sequence favors repetition rates faster than those of direct ^{13}C detection, and hence, an increase in the signal-to-noise ratio per unit time can be obtained.

To investigate the different effects of relaxation processes on the detected signal, three different segments are distinguished within the sequence: During the forward and backward polarization transfers, relaxation takes place in the doubly rotating frame. For the sake of simplicity we assume a single time constant $T_{\rho,\mathrm{eff}}^{-1} = \frac{1}{2}(T_{1\rho}^{-1} + T_2^{-1})$ for both the forward and the backward transfer. The reasoning of this representation of $T_{\rho,\mathrm{eff}}$ originates from the fact that half of

the magnetization remains spin locked ($\sigma \approx (I_x + S_x)$, decay rate $T_{1\rho}^{-1}$) while the other half nutates under the effective coupling ($\sigma \approx (I_x - S_x)$, decay rate $T_{2\rho}^{-1} \approx T_2^{-1}$). The actual relaxation behavior during this part of the sequence depends on the type of polarization transfer and on possible cross relaxation processes, and hence, our assumption will be an oversimplification. In the second part of the sequence, during the period of the proton saturation ($T_{\mathrm{Sat.}}$), the desired coherence is stored along the positive (or negative) z axis and is relaxing longitudinally toward the S spin equilibrium magnetization with the time constant $T_{1,S}$ of the ^{13}C nucleus. In the third and last part, during the repetition delay T_R, longitudinal proton relaxation takes place with the time constant $T_{1,I}$.

Therefore, the time-dependent evolution of the density matrix, including relaxation processes, can be written as

$$\sigma_{I_NS}(2\tau, T_{\mathrm{Sat.}}, T_R) = \sigma_{I_NS}^f(2\tau)\exp\left(-\frac{2\tau}{T_{\rho,\mathrm{eff}}}\right)$$

$$\times \left(\frac{\gamma_S}{\gamma_I}\,\begin{matrix}+\\(-)\end{matrix}\left(1\,\begin{matrix}-\\(+)\end{matrix}\,\frac{\gamma_S}{\gamma_I}\right)\exp\left(-\frac{T_{\mathrm{Sat}}}{T_{1,S}}\right)\right)$$

$$\times \left(1 - \exp\left(-\frac{T_R}{T_{1,I}}\right)\right) \quad [15]$$

using the expressions for $\sigma_{I_NS}^f(2\tau)$ given in Eqs. [8], [9], and [10]. $T_{\mathrm{Sat.}}$ is the required duration for the complete saturation of proton spins, and the selected coherence is assumed to be stored along the positive (negative) z axis. Typically $T_{\mathrm{Sat.}}$ is much smaller than $T_{1,S}$. T_R is the repetition time between two successive transients.

Equation [15] can be used to calculate the optimum contact times for the three different spin systems. For the IS and the I_2S systems analytical solutions exist

$$\tau_{\mathrm{opt}} = \tau_0\,\frac{2}{\pi}\,\arctan\left(\pi\,\frac{T_{\rho,\mathrm{eff}}}{\tau_0}\right) \quad [16]$$

and τ_0 given by Eq. [11]. For the I_3S spin system the solution must be calculated numerically.

By using Eqs. [15] and [16], the resulting signal strength for the three different spin systems can be obtained. Figure 2 shows the signal strength as a function of $T_{\rho,\mathrm{eff}}$ and $T_{1,I}$. Values of $T_{\rho,\mathrm{eff}}$ have been chosen in the range of $T_{2,I} \leq T_{\rho,\mathrm{eff}} \ll T_{1,I}$. T_R was kept constant at 500 ms, a fixed ratio of $T_{\mathrm{Sat.}}/T_{1,S} = 0.2$ was assumed, and J values were set to 169, 144, and 120 Hz for the IS, I_2S, and the I_3S system, respectively. This choice of parameters corresponds to typical values which we encountered in our experiments.

From Fig. 2 it is obvious that short values of $T_{\rho,\mathrm{eff}}$ have a strong attenuating effect on the signal. This is most pronounced for small spin systems due to the longer contact times required. The dependence of the signal strength on $T_{1,I}$ and T_R is the same for conventional proton spectroscopy
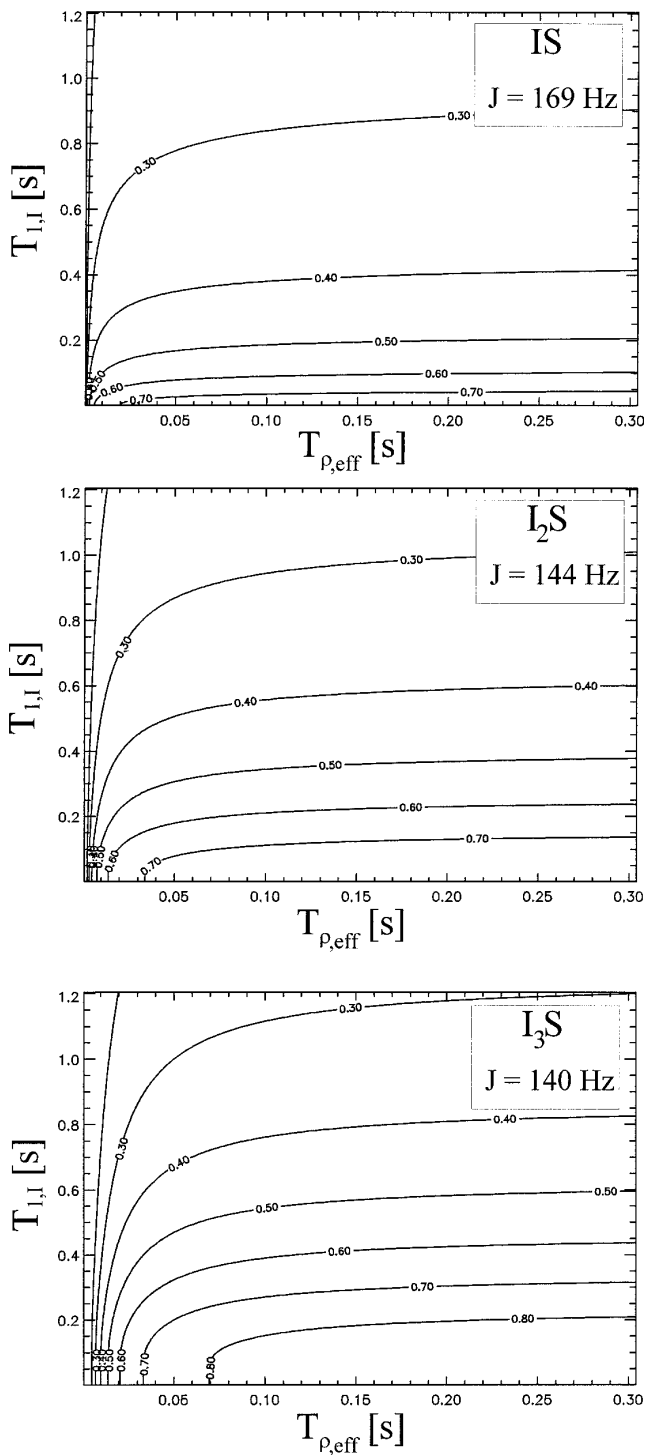
FIG. 2. Simulated signal strength produced by CYCLCROP for IS, I_2S, and I_3S spin systems as a function of relaxation times. $T_{1,I}$ is the longitudinal relaxation time for protons, and $T_{\rho,\text{eff}}$ the effective relaxation time during polarization transfers (see text). The values given in the figures are normalized to the maximum signal which can be obtained for the IS system. J coupling constants have been chosen as 169, 144, and 140 Hz for the IS, I_2S, and the I_3S spin system, respectively. The repetition time T_R is 500 ms, a typical value used in our experiments.

or imaging, apart from the fact that the Ernst angle (22) cannot be used to increase the signal-to-noise ratio per time interval because of complete proton saturation between the forward and backward polarization transfer.

Our considerations demonstrate that the full signal enhancement can only be achieved for long T_R and $T_{\rho,\text{eff}}$. In most cases, the dependence of the signal strength on the contact times τ_{opt} as a function of the spin system size makes larger spin systems more favorable. For quantitative studies, precise knowledge of the various relaxation times is therefore indispensable.

In the imaging experiment, Eq. [15] must be extended by an additional relaxation factor of $e^{-T_E/T_{2,I}}$, arising from transverse relaxation of the selected coherence during the intervall T_E of the spin echo. Hence, image contrast depends (i) on the local concentration of the selected molecule and (ii) on spatial variations of the relaxation parameters of the molecule, namely $T_{1,I}$, $T_{2,I}$, $T_{\rho,\text{eff}}$, and $T_{1,S}$. By an appropriate choice of the imaging parameters, the influence of $T_{1,I}$ and $T_{2,I}$ relaxation on the image contrast can be kept low. However, significant contrast created by relaxation processes in the doubly rotating frame cannot be avoided whenever the spatial variation of $T_{\rho,\text{eff}}$ within the sample is high and when $T_{\rho,\text{eff}}$ itself is of the order of the required contact time τ_{opt}. Note that in principle the dependence of the signal strength on $T_{1,S}$, the longitudinal relaxation time of the ^{13}C nucleus, offers the possibility of creating contrast caused by spatial variations of molecular dynamics at four times lower than the detection frequency. In most cases, the duration which is required for the saturation of nonselected proton coherences is typically much smaller than T_1 values of the ^{13}C nucleus, and therefore this image contrast can easily be kept negligible.

The precise knowledge of relaxation times enables the correction of the CYCLCROP imaging data to obtain quantitative maps of the concentration of a single molecule within the sample.

EXPERIMENTAL

All *in vivo* experiments were carried out using a Bruker Avance DSX 400 digital spectrometer, equipped with a 9.4-T superconducting wide-bore magnet and actively screened gradients. For excitation and signal detection, a custom-built double resonant saddle coil was used, with the two resonances tuned to proton and carbon frequencies, which are 400 and 100 MHz, respectively. The coil has a diameter of 7 mm and is 15 mm long. Typically, the lengths of the $\pi/2$ pulses were 19 μs for proton excitation and 45 μs for carbon excitation. The region within the coil in which the polarization transfer is effective is 5 mm in diameter and 12 mm in length, as measured by test samples consisting of ^{13}C-enriched methanol in water (25% v/v).

The probehead accommodated a glass tube, 14 mm in diameter and 180 mm length, containing the seedling's roots
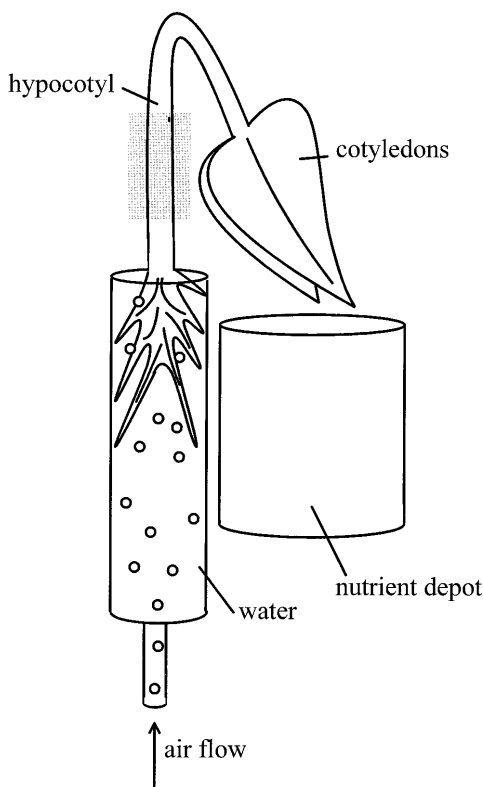
FIG. 3. Experimental setup for indirect ^{13}C NMR observation of uptake and transport of labeled hexoses in plants. Castor bean seedlings have been grown on top of a glass tube outside the magnet for six days in darkness. The glass tube can be inserted into the probehead. During the experiment, the root system of the plants was aerated from below by a gentle stream of air bubbles. At the beginning of the experiment, the endosperm of the cotyledons was removed. During the experiment, the cotyledons were incubated in a small nutrient depot containing 50 mM ^{13}C$_1$ glucose and 50 mM ^{13}C$_1$ fructose in 5 mM HEPES buffer of pH 5.5. The shaded region within the hypocotyl indicates the position of the NMR RF coil.

(Fig. 3). Castor bean seedlings were grown hydroponically on top of such tubes outside the RF coil for six days in darkness. The germination and conditions for growth are as described in (3). During the experiment, the root system of the plants was aerated from below by a gentle stream of air bubbles. The temperature of the probehead could be measured and controlled from outside the magnet and was kept constant at 300 K. Before the beginning of the experiment, the endosperm of the cotyledons was removed. Throughout the experiment, the cotyledons were incubated in a small nutrient vessel containing a solution of ^{13}C-labeled hexoses, namely 50 mM ^{13}C$_1$ glucose and 50 mM ^{13}C$_1$ fructose in 5 mM HEPES buffer of pH 5.5.

Polarization transfer was achieved by using the MOIST sequence. The spin lock and contact pulse radiofrequency field strengths were matched at $\omega_1/2\pi = 4$ kHz, and we choose 12 phase inversions for each transfer. Proton spins were saturated using four adiabatic half passages, each followed by a single gradient crusher pulse, giving a total duration for saturation of 40 ms. The CYCLCROP sequence was followed either by a selective π pulse with a slice gradient to produce slice selective spin echoes or by a spin echo imaging sequence without any slice selection.

In the case of slice selective edited spectra, the echo time was $T_E = 2$ ms, and only the second half of the echo was acquired. Slice selection can also be achieved by applying gradients during the periods of the polarization transfers (7, 15, 16). The advantage of the variant which we used here is an easy verification of the position and the shape of the selected slice by conventional proton slice profiles using the same soft pulses and gradient strength. In the case of imaging experiments, the slice thickness is set by the effective volume for polarization transfer in the coil (12 mm). The echo time for imaging was set to $T_E = 4$ ms and the complete echo was acquired.

Cleavage of sucrose within the plant results in the production of the two hexoses, fructose and glucose. High resolution spectra of these compounds show that only the resonance of the C1 molecular group of free fructose is in close proximity to the C1′ resonance of the sucrose (the C1 of the fructose moiety within the sucrose molecule, termed as F1 in the following, see Fig. 4). To demonstrate that these two resonances are distinguishable in our experiments, a 5-mm NMR sample tube divided into two compartments was
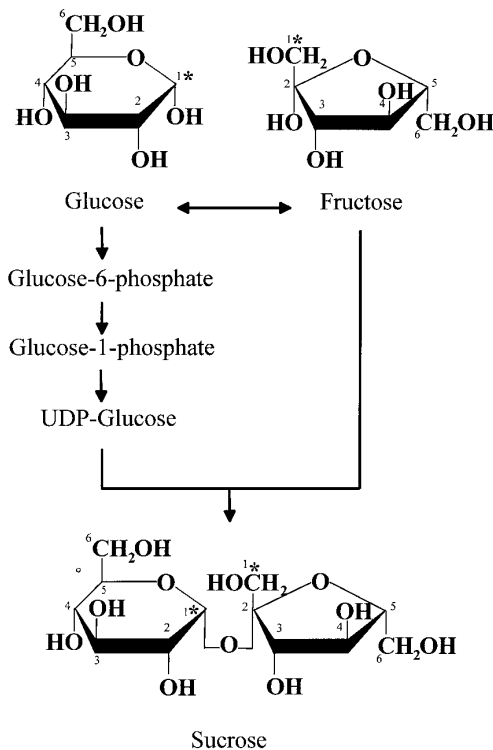
FIG. 4. The sucrose molecule. NMR resonances which arise from protons J coupled to ^{13}C nuclei at the C1′ position of sucrose (fructose moiety) will be termed the *F1 resonance of sucrose,* and resonances from protons which are coupled to ^{13}C nuclei at the C1 position (glucose moiety) will be termed the *G1 resonance of sucrose.*

filled with solutions of sucrose and fructose in D_2O (830 mM at natural ^{13}C abundance). Profiles along the z axis of this tube were recorded with the proton and ^{13}C frequencies set to the F1 resonance of sucrose and the C1 group of free fructose. Each profile is the result of 1024 scans with a repetition delay of 500 ms.

The experimental protocol used to perform dynamic studies of sucrose metabolism and transport in the castor bean seedling consisted of the following steps: (i) Edited spectra of the F1 resonance of sucrose and of the protons coupled to the C1 of the sucrose is recorded (the C1 of the glucose moiety within the sucrose molecule, termed as G1 in the following, see Fig. 4). These measurements were performed with ^{13}C nuclei in natural abundance. (ii) The incubation of the plant is started using the ^{13}C-labeled hexoses. (iii) Decoupled spectra of the F1 and G1 resonances of sucrose with and without slice selection are alternately recorded over a period of 8 h. Each of the spectra is the result of 256 accumulations which were taken within 3 min, interleaved by a time interval of 30 min. A total of 1024 data points were acquired, the spectral width was 8 kHz, and the repetition time was set to 500 ms.

Before Fourier transformation, a 20-Hz exponential line broadening was applied, followed by zero filling to 2k complex data points. (iv) Finally the spatial distribution of the labeled sucrose is mapped via the F1 resonance. For this purpose, a spin echo imaging sequence ($T_E = 4$ ms) was added to the CYCLCROP editing sequence. Each of the images is the result of the acquisition of a 128×16 complex data matrix. The field of view is 7 mm for both transverse directions, and the slice width is given by the length of the sensitive volume of the coil (12 mm). To achieve a sufficiently high signal-to-noise ratio, 600 scans were accumulated for each phase-encoding step. With a repetition time T_R set to 500 ms, this results in a total measurement time of 1.5 h. The raw data were processed with a matched Hanning filter and zero filled to 128×128 complex points prior to 2D Fourier transformation. The digital resolution of these images is 55 μm $\times$ 438 μm.

High resolution heteronuclear correlation spectroscopy with a 100-mM sucrose solution in 99.8% D_2O was performed on a Bruker Avance DPX 400 NMR spectrometer. The high resolution probe consists of two orthogonal saddle coils with typical $\pi/2$ pulse lengths of 10 μs for protons and 6.7 μs for the ^{13}C nuclei.

Proton relaxation times of the 100-mM sucrose solution were measured with the DSX 400 spectrometer. Saturation recovery and inversion recovery techniques were used for proton longitudinal relaxation time measurements. Both techniques yield comparable results. T_1 relaxation times were calculated from 32 data points which have been obtained from different recovery times ranging between 10 ms and 4.8 s. Transverse proton relaxation times were measured using the CPMG sequence with a fixed delay of 3.3 ms between two consecutive refocusing pulses. Signals arising from 32 different total echo times between 10 and 330 ms were measured. The resulting signals for the F1 and G1 resonances of sucrose were integrated and fitted to single exponential decays.

RESULTS

In order to obtain precise values of the carbon and proton frequencies of the coupled spin pairs, a high resolution heteronuclear correlation spectrum of a 100-mM sucrose solution in 99.8% D_2O was recorded (Fig. 5). From this spectrum, the proton–carbon connectivity for the different molecular groups can be derived. With the residual water line as a reference, this spectrum serves as a primary starting point for correct frequency selection in the *in vivo* experiment with the seedlings. Table 1 summarizes the chemical shifts, J coupling constants and the relaxation times for the two positions G1 and F1, measured in the sucrose solution. The longitudinal relaxation times for the ^{13}C nucleus are taken from (23). We expect to observe enrichment of the ^{13}C nuclei at both positions in the sucrose molecule if labeled hexoses ($^{13}C_1$ glucose and $^{13}C_1$ fructose) are taken up by the cotyledons and are used for sucrose synthesis.

Figure 6 shows the *in vivo* proton spectrum from the hypocotyl of the seedling. The magnetic field homogeneity was optimized over the whole sensitive volume of the coil, to give a water linewidth at half-height of about 70 Hz. The G1 sucrose resonance at 5.30 ppm is not resolved and is covered by the broad base of the water resonance line. The F1 sucrose resonance (3.56 ppm) is poorly resolved and appears as a broad peak together with other sucrose resonances between 3.0 and 4.5 ppm. In the region between 2 and 2.4 ppm, the overlapping resonances of the amino acids glutamine, glutamate, and arginine are detected.

Taking the water line as reference, the correct proton frequencies of F1 and G1 in the *in vivo* experiment with the seedling can be selected by looking up the frequencies from the heteronuclear correlation spectrum. The corresponding carbon frequencies are measured from a standard ^{13}C spectrum, recorded once from the hypocotyl of the seedling. CYCLCROP spectra without slice selection of the F1 and G1 resonances of sucrose were acquired with 240 scans within 3 min (Figs. 7A and 7B). In each figure, three CYCLCROP spectra are provided: (1) the edited spectrum with ^{13}C continuous wave decoupling, (2) the J-coupled spectrum, and (3) a spectrum from an experiment in which the ^{13}C radiofrequency power of the spin lock and contact pulses on the carbon side were Hartmann/Hahn mismatched by attenuating the power level on the carbon RF channel by 10 dB. The third spectra clearly demonstrate the absence of any residual signals which could possibly arise from imperfect saturation of the proton spins. Therefore, the signals in spectra (1) and (2) of Fig. 7 are solely created by the cyclic polarization transfer of the editing sequence. Note that this method allows the complete suppression of unwanted signals
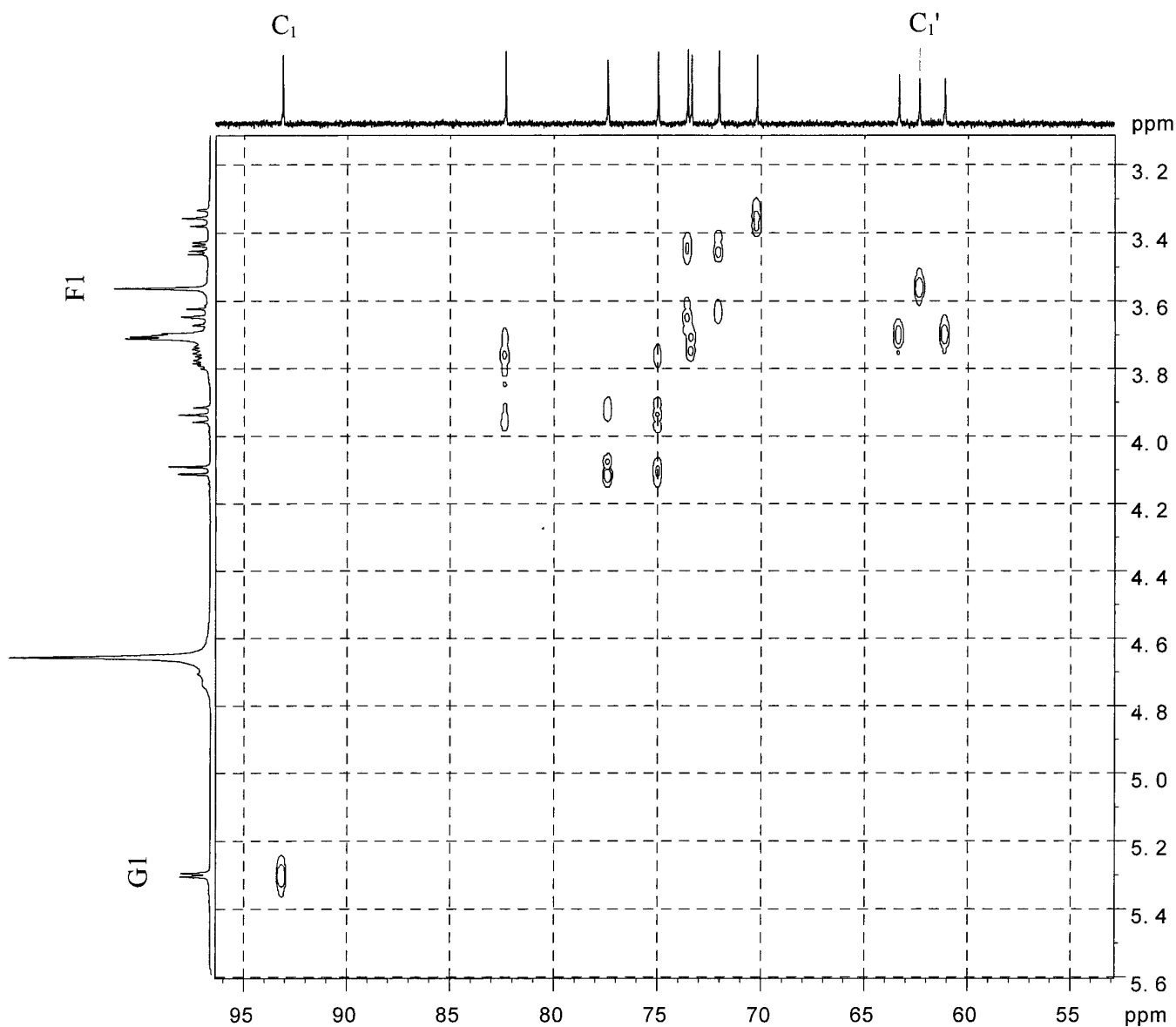
FIG. 5. High resolution 2D heteronuclear correlation spectrum of a 100 mM sucrose solution in 99.8% D_2O, recorded at 400 MHz. From this spectrum, the proton and carbon connectivity of the different molecular groups of sucrose can be derived. The F1 and G1 resonance frequencies of sucrose are indicated, and they serve as a starting point for the experiment in the living castor bean seedling.

arising from the water resonance, as well as signals from protons not coupled to the selected ^{13}C nucleus.

Figure 8 demonstrates the high frequency selectivity of the CYCLCROP sequence. It shows profiles generated from a phantom consisting of two compartments, one containing 830 mM fructose in D_2O, the other a similar solution of sucrose. The upper profile was recorded with the RF frequencies set to 62.3 ppm (^{13}C) and 3.56 ppm (^1H), the C1'/F1 resonances of sucrose. For the lower profile, we used the corresponding frequencies of the C1 molecular group of free fructose (64.8 and 3.63 ppm). Despite the small difference in ^{13}C frequencies, in both cases, only the selected compartment was detected.

In our experiments on the castor bean seedlings we recorded spectra from three different slices in order to observe transport of sucrose along the hypocotyl axis. Each slice is 2 mm thick, and adjacent slices are separated by 4 mm. This slice selection process causes almost no loss in signal intensity, as a comparison of the edited profile along the axis of the hypocotyl with the signal intensities of the three slice profiles demonstrates (Fig. 9). These profiles were recorded after 8 h of incubation with labeled hexoses.

For the dynamic study of the uptake of the labeled hexoses ($^{13}C_1$ glucose and $^{13}C_1$ fructose), their conversion to sucrose and the transport of sucrose along the hypocotyl of the seedling, the increase in intensities of the F1 and G1 resonances was

TABLE 1
Summary of NMR Properties of C1 and C1′ Hydrocarbon Groups of Sucrose

	$\delta(^1H)$ (ppm)	$\delta(^{13}C)$ (ppm)	J (Hz)	$T_1(^1H)$ (ms)	$T_2(^1H)$ (ms)	$T_1(^{13}C)$ (s)
F1/C1′	3.56	62.3	144	352	248	1.75
G1/C1	5.30	93.1	169	778	182	1.03

observed for 8 h. The spectra were acquired without (Fig. 10) and with (Fig. 11) slice selection. The three different positions of the slices are the same as those indicated in Fig. 9. The integrated and normalized (to maximum F1 intensity) intensities of the F1 and G1 resonances of sucrose are plotted in Fig. 11. In the acquisition of the F1 resonance of the central slice ($z = 0$), the proton frequency was misset deliberately and no signal was detected due to Hartmann/Hahn mismatch. As with spectra (3) of Fig. 7, this demonstrates that the signal in the CYCLCROP sequence arises only from resonances of molecular groups which have followed the cyclic coherence pathway. The enrichment of labeled sucrose in the observed region of the hypocotyl, as calculated from the increase in signal intensities of the F1 and G1 resonances, is almost linear for the first
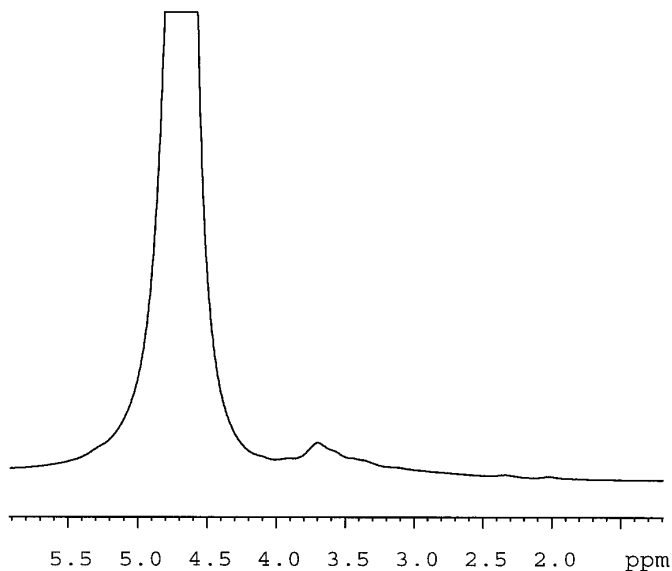
FIG. 6. *In vivo* proton spectrum from the hypocotyl of a 6-day-old castor bean seedling with no explicit slice selection (the slice thickness is set by the sensitive volume of the coil at 12 mm). The magnetic field homogeneity was optimized over the sensitive volume of the coil to give a water linewidth at half-height of about 70 Hz (acquisition parameters are spectral width = 8 kHz, number of points = 2k, zerofilling to 4k complex points, number of scans = 4, T_R = 3 s). The G1 resonance of fructose at 5.3 ppm is not resolved and is covered by the broad base of the water resonance line. The F1 resonance of sucrose is poorly resolved and appears as a broad peak together with other sucrose resonances between 3.0 and 4.5 ppm. In the region between 2 and 2.4 ppm the overlapping resonances of the amino acids glutamine, glutamate, and arginine are detected.
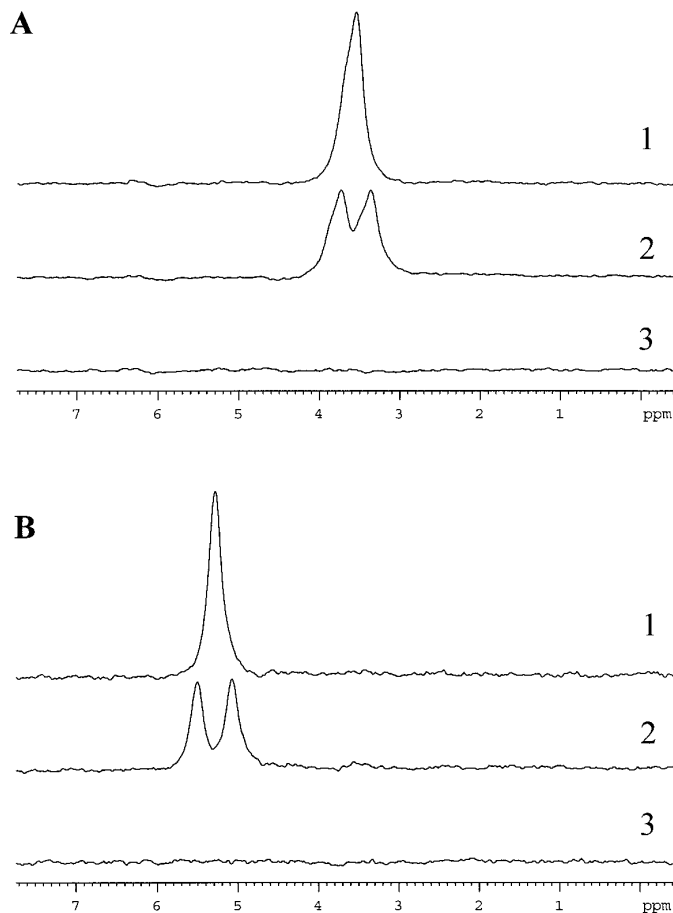
FIG. 7. *In vivo* CYCLCROP spectra from the hypocotyl of a 6-day-old castor bean seedling with no explicit slice selection (the slice thickness is set by the 12-mm length of the sensitive volume of the coil). The frequencies are set according to the F1 (A) and G1 (B) resonance frequencies of sucrose. Each of the two sets shows three spectra. Spectrum (1) was recorded with continuous wave decoupling, and spectrum (2) shows the J splitting of protons which are coupled to the selected ^{13}C nucleus. In order to demonstrate the absence of any residual signals which do not belong to the selected carbohydrate group, the SL and CP pulse power levels on the carbon side have been attenuated (and therefore Hartmann/ Hahn mismatched) by 10 dB in spectrum (3). This proves that signals in spectra (1) and (2) solely arise from coherences which have followed the cyclic polarization transfer editing process. Note the complete suppression of the water resonance line. The FID was recorded with 1024 data points and a sweep width of 4 kHz. Prior to Fourier transformation, the FID was processed with an exponential filter (20 Hz line broadening) and zero filled to 2k complex data. A total of 240 scans were accumulated with a repetition delay T_R = 400 ms.

six hours; afterward the rate decreases. The absolute intensities as well as the rate of increase differ at the three positions within the stem. This result was observed for both the F1 and the G1 resonances.

In order to monitor the spatial distribution of the labeled sucrose in the hypocotyl of the seedling, spin density maps of the F1 resonance of sucrose were acquired and are shown in Fig. 12. We conclude from our experiment with the two-compartment tube (Fig. 8) that the signal in this imaging
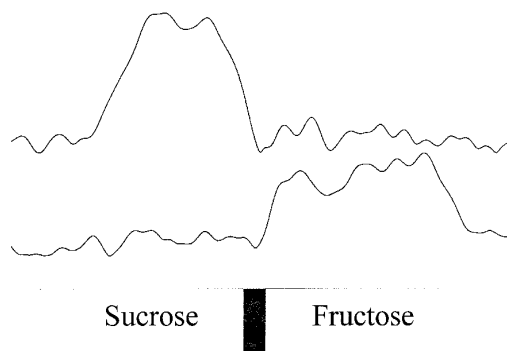
FIG. 8. CYCLCROP profiles of a sample which contains a solution of fructose in D_2O (right half) and a solution of sucrose in D_2O (left half), each of them 830 mM and at natural ^{13}C abundance. The lower profile was recorded using the carbon and proton resonances of the C1 molecular group of fructose ($\delta(^{13}C) = 64.8$ ppm, $\delta(^{1}H) = 3.63$ ppm), and the upper profile with frequencies set according to the F1 resonances of the sucrose molecule ($\delta(^{13}C) = 62.3$ ppm, $\delta(^{1}H) = 3.56$ ppm). Both profiles were accumulated 1024 times with a repetition delay of 500 ms.

experiment originates unambiguously from the F1 resonance of the synthesized sucrose and that any contributions of free fructose can be excluded. The resolution of these maps is $55\ \mu m \times 438\ \mu m$; the slice thickness is given by the sensitive volume of the coil (12 mm).

As a reference, a conventional high resolution proton image from a slice within the hypocotyl was taken using a T_1-weighted spin echo NMR imaging sequence (echo time = 8 ms, repetition time = 300 ms). The use of 256×256 complex data points together with a 7-mm FOV gives a nominal resolution of $27\ \mu m$ within the 1-mm slice. The proton images and carbon spin density maps of the F1 resonance of sucrose shown in Fig. 12 were taken from two different seedlings, after 8 h of incubation. Figures 12A and 12B were generated from the first seedling, Figs. 12C and 12D from the second. In Fig. 12D the conventional proton image has been overlaid on the carbon image as a contour plot. Both edited carbon images show a comparable distribution of sucrose within the hypocotyl. The vascular bundles cannot be resolved in detail in the ^{13}C images, but these images show higher intensity at positions which correspond to the sites of the vascular bundles. The poor resolution arises from imperfect longitudinal symmetry of the stem in combination with the lack of slice selection.

As has been shown in the slice profiles above, slice selection is possible, but at the expense of a considerable increase of measurement time. Differences in the signal intensities within the hypocotyl might be a consequence of imperfect centering of the plant within the coil, but this effect should also have shown up in the normal proton images. They might also indicate different local transport activity either within the vascular bundles or the surrounding parenchyma.

DISCUSSION

We have applied indirect ^{13}C spectroscopy and imaging techniques, based on cyclic polarization transfer to the inves-

tigation of sucrose metabolism and transport in six-day-old castor bean seedlings. These noninvasive techniques enable us to observe the undisturbed situation in the intact plant. ^{13}C-labeled compounds are especially attractive for studies of metabolic pathways and transport processes in living systems since (i) the low natural abundance of ^{13}C nuclei favors their use as tracers and (ii) the wide range of ^{13}C chemical shifts allows their easy identification. The drawback of direct ^{13}C NMR detection is the relatively weak NMR sensitivity of the ^{13}C nucleus which requires either a large number of ^{13}C nuclei within the sample or long experimental times. In addition, the long spin–lattice relaxation times of the ^{13}C nucleus prevent rapid signal accumulation.

CYCLCROP combines three advantages: (i) the wide range of ^{13}C chemical shifts enables high spectral selectivity, (ii) indirect detection of ^{13}C nuclei provides the high sensitivity of proton NMR, and (iii) complete suppression of all proton resonances which do not arise from the desired molecular groups is achieved. The profiles in Fig. 8 as well as the spectra of F1 and G1 shown in Fig. 10 provide striking examples of the power of this technique. The first spectra in these sets were acquired from the sucrose in the seedling (≈ 100 mM) with ^{13}C in natural abundance ($\approx 1.1\%$) within an experimental time of only 3 min. The high spectral selectivity of the CYCLCROP sequence is demonstrated by the profiles of Fig. 8. Despite the small differences of the ^{13}C and proton resonance frequencies between the C1 in the free fructose and the C1' of the fructose moiety of sucrose and their attached proton, the distribution of both molecules can be distinguished. Because of the high spectral selectivity, a prerequisite for the application of the sequence is a precise knowledge about the nature of the chemical compound under
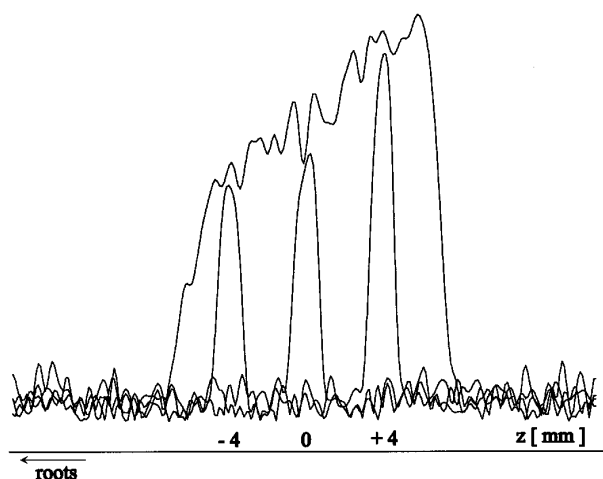
FIG. 9. *In vivo* positions of slices, monitored by F1-edited profiles along an axis parallel to the hypocotyl of the seedling. In the case of edited slice profiles, an additional slice gradient was applied during the frequency-selective refocusing π pulse. All profiles were taken 8 h after the beginning of incorporation of ^{13}C-labeled hexoses ($^{13}C_1$ fructose and $^{13}C_1$ glucose). Acquisition parameters were FOV = 30 mm, NS = 512, $T_R = 500$ ms, number of points = 128, zero filling to 256 complex points, $T_E = 4$ ms.
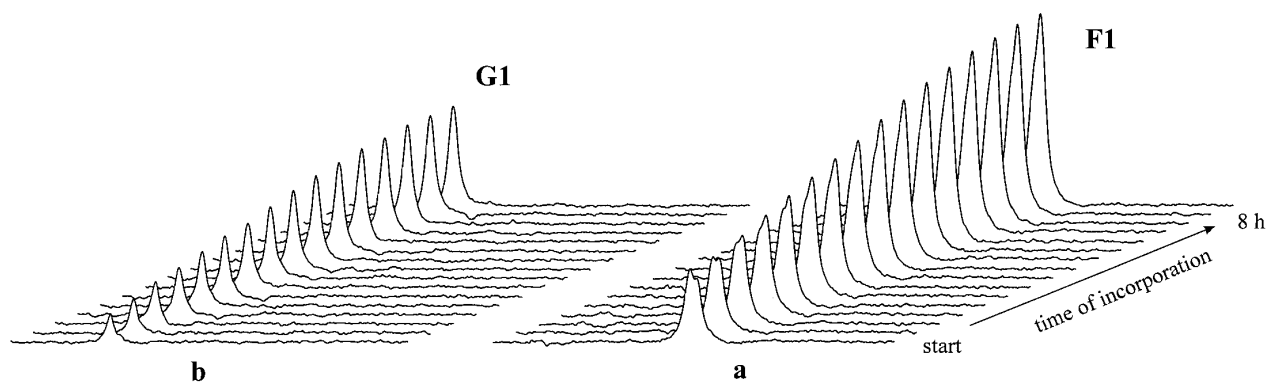
FIG. 10. Enrichment of ^{13}C-labeled sucrose as a result of uptake of ^{13}C-labeled hexoses ([13]C_1 fructose and [13]C_1 glucose) and their conversion to sucrose which is ^{13}C-labeled at the C1′ position of the fructose moiety (a) and at the C1 position of the glucose moiety (b). The stacked plots show the increasing intensities of the F1 and G1 resonances as a function of the incubation time. Each of these spectra is the result of 256 scans which were accumulated within 3 min from the hypocotyl of 6-day-old castor bean seedlings without explicit slice selection (the slice thickness is given by the 12-mm sensitive volume of the NMR coil). Consecutive spectra are separated by a time interval of 30 min (spectral width = 8 kHz, number of points = 1024, T_R = 500 ms, 20 Hz exponential line broadening, zero filling to 2048 complex points).

investigation. This information can be either obtained by direct ^{13}C spectroscopy or by 2D heteronuclear correlation spectroscopy.

CYCLCROP offers the major advantage of allowing rapid acquisition of indirectly detected ^{13}C spectra of the selected molecular groups. Because a high time resolution can be achieved, the ^{13}C-based technique can be used to follow the tracer flux through metabolic pools in a time-resolved study. By combining CYCLCROP with frequency and phase-encoding NMR imaging techniques, highly specific information about the time-dependant evolution and distribution of a single ^{13}C label within a selected molecule can be visualized in a spin density map.

In summary, CYCLCROP ^{13}C spectroscopy or imaging of metabolites in plants relies on a tracer strategy. It permits visualization and quantification of specific metabolic and transport activities which involve the ^{13}C-labeled tracer and which occur while the system under investigation itself is in an almost unperturbed equilibrium state. This unique information content of the experiment makes it very distinct from the CSI or COSY-type experiments reported earlier (4, 10). In those experiments it is possible to create simultaneously images of a variety of different metabolites during a static situation of the plant, assuming the required high spectral resolution can be achieved *in vivo*.

By the correct choice of experimental parameters it is possible to create contrast in the image which depends mainly on the spatial variations of the spin density within the sample. However, it can be concluded from the simulations of the signal strength (Fig. 2) that for $T_{\rho,eff}$ values on the order of the required contact times, signal attenuation due to relaxation effects cannot be avoided. Even in this case the technique can nevertheless be quantitative by post processing based on the separately determined relaxation times of the selected molecular groups.

In many plant species, large magnetic susceptibility differ-ences arise from high concentrations of intercellular air spaces. They lead to a spread of the local Larmor frequencies and local variations of T_2^* values through molecular diffusion between regions of different resonance frequencies. Rotating frame experiments may be affected by susceptibility effects through two different kinds of processes: (i) by local Hartmann/Hahn mismatch which relates to both B_0 and B_1 effects; and (ii) by local short values of $T_{\rho,eff}$. In the present study, a comparison between the linewidth of edited and nonedited resonances suggests that with our single-coil probe selective J cross polarization efficiency bears no evidence of Hartmann/Hahn mismatch effects. However, a local reduction of transverse relaxation times (T_2 effect) (24) through molecular diffusion in the presence of strong internal field gradients will also reduce the local $T_{\rho,eff}$ value and precaution must be paid in the quantitative interpretation of CYCLCROP images within regions which are known to be severely affected by susceptibility artifacts. From the reference proton image of the hypocotyl of the castor bean seedling and given the somewhat coarse-grained resolution we achieved in our experiments we are unable to infer any strong susceptibility influences.

In these experiments we supplied [13]C_1 fructose and [13]C_1 glucose to the cotyledons of the castor bean seedling. We observed uptake of the labeled hexoses supplied and their conversion to the disaccharide sucrose. Sucrose is the product of the enzymatically catalysed condensation between fructose and uridine-diphosphate glucose (UDP glucose). UDP-glucose is synthesized from glucose via phosphorylation and exchange of the phosphate group by UDP. Free fructose can be isomerized by the enzyme hexose isomerase to free glucose (Fig. 3). Both hexoses are taken up by carrier proteins which are located in the cell plasmamembrane.

The analysis of the time course study of the increase in intensity of both the F1 and the G1 resonances in a selected slice of the hypocotyl shows three notable features: (i) the
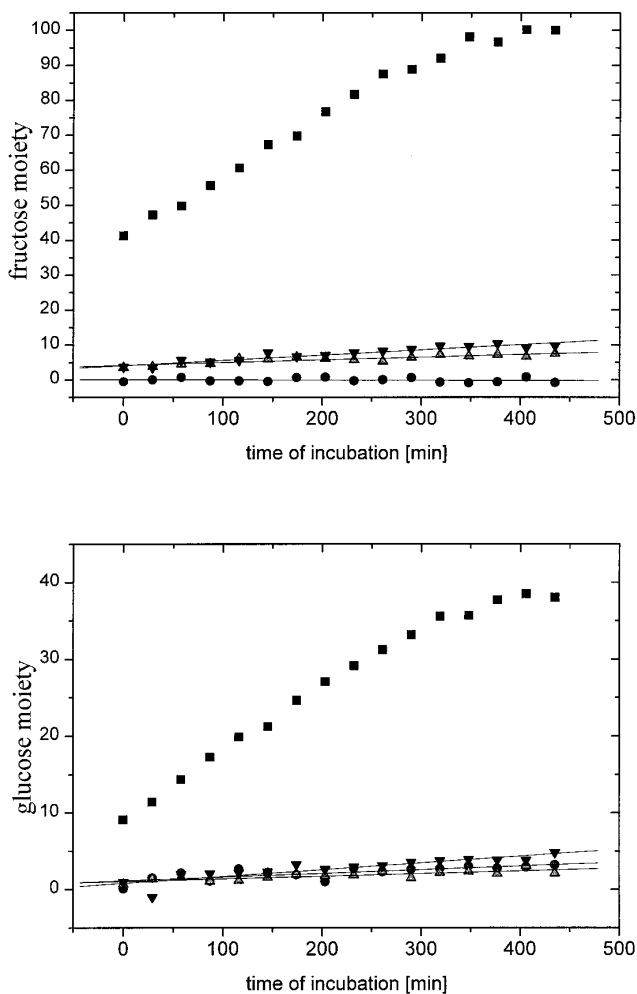
FIG. 11. The graphs show the time-dependent enrichment of ^{13}C-labeled sucrose after uptake of ^{13}C-labeled hexoses ($^{13}C_1$ fructose and $^{13}C_1$ glucose), conversion to sucrose, and its transport to the hypocotyl. The synthesized sucrose is labeled at the C1′ and C1 position, corresponding to the fructose and glucose moieties, respectively. The resonances arising from protons which are *J* coupled to these sites give rise to CYCLCROP-edited signals, the F1 and G1 resonances of sucrose, respectively. Data points (■) represent the normalized integrals of the F1 and G1 resonances of sucrose without slice selection. For both resonances, signals were also recorded from slices perpendicular to the hypocotyl of the seedling at positions of −4 mm (▲), 0 mm (●) and +4 mm (▼), see Fig. 9. In the acquisition of the F1 resonance of sucrose from the central slice, the ^1H frequency was misset deliberately, and therefore no signal was detected.

absolute intensity of the F1 resonance is always higher than that of the corresponding G1 resonance; (ii) the ratio of these intensities changes during the time course of the experiment; and (iii) the observed increase in intensities for the F1 and G1 resonances differs for each of the three selected slices.

One reason for the difference in absolute intensity is the influence of relaxation on the detected CYCLCROP signal strength. It can be seen from the relaxation time measurements of sucrose in solution that the proton T_1

relaxation time of the F1 resonance is considerably shorter than the corresponding G1 longitudinal relaxation time. This allows faster repetition rates for the F1 resonance of sucrose to achieve the optimum ratio of signal-to-noise per time interval.

On the other hand, the transverse relaxation times of the two resonances show opposite behavior with the G1 resonance relaxing faster than the F1 resonance (Table 1). Since we were using the same repetition delays for both observed resonances of sucrose, the observed signal arising from the G1 resonance is less intense than that arising from the F1 resonance of sucrose. In addition, relaxation losses during the two polarization transfers are less important for the F1 resonance of sucrose than for the G1 resonance because (i) the contact times for the F1 resonance are shorter and (ii) the effective relaxation time $T_{\rho,eff}(F1)$ is longer than that for the G1 resonance.

At present, no data for the relaxation times *in vivo* are available and therefore no intensity ratio can be calculated from Eq. [15]. However, we assume that the observed relaxation processes in the sucrose molecule are similar under *in vivo* conditions. To give an order of magnitude estimate, the relaxation times from Table 1 together with a repetition delay of 500 ms indicate a ratio of 1:0.61 (Fig. 2). This ratio has been verified in the sucrose test solution.

It is at present uncertain whether relaxation effects can fully explain the measured ratio of ≈1:0.4 between the intensities of the F1 and G1 resonances of sucrose in the seedling at the end of the experiment. This observation might also be explained by a preferential use of one of the supplied hexoses for the synthesis of sucrose. This explanation is also supported by the second effect we observed. The ratio between the intensities of F1 and G1 of sucrose is not constant during the time course of the experiment. We observed a ratio between the F1 and G1 intensities of sucrose of 1:0.2 at the beginning, whereas this ratio is 1:0.4 after 8 h of incubation with ^{13}C-labeled hexoses. If the two hexoses (glucose and fructose) are equally used for the synthesis of sucrose, this ratio should not change in time. In our experiment the change in the time course can be explained by a preferential use of the supplied ^{13}C fructose for the synthesis of sucrose at the beginning of the experiment. Toward the end of the experiment, fructose and glucose are equally built into the sucrose molecule.

The reason for the observed differential incorporation of the two supplied hexoses into sucrose is at the moment unknown. Kallarackal and Komor (*25*) described that fructose is preferentially used for the synthesis of sucrose, since sucrose concentration in the phloem sap can be kept high by a sufficiently high supply of fructose to the cotyledons. If glucose is supplied in a comparatively high concentration, only the glucose concentration in the phloem sap increases while the sucrose concentration remains low. Kallarackal and Komor (*25*) suggested that fructose is not absorbed well by the phloem, but instead preferentially absorbed by the
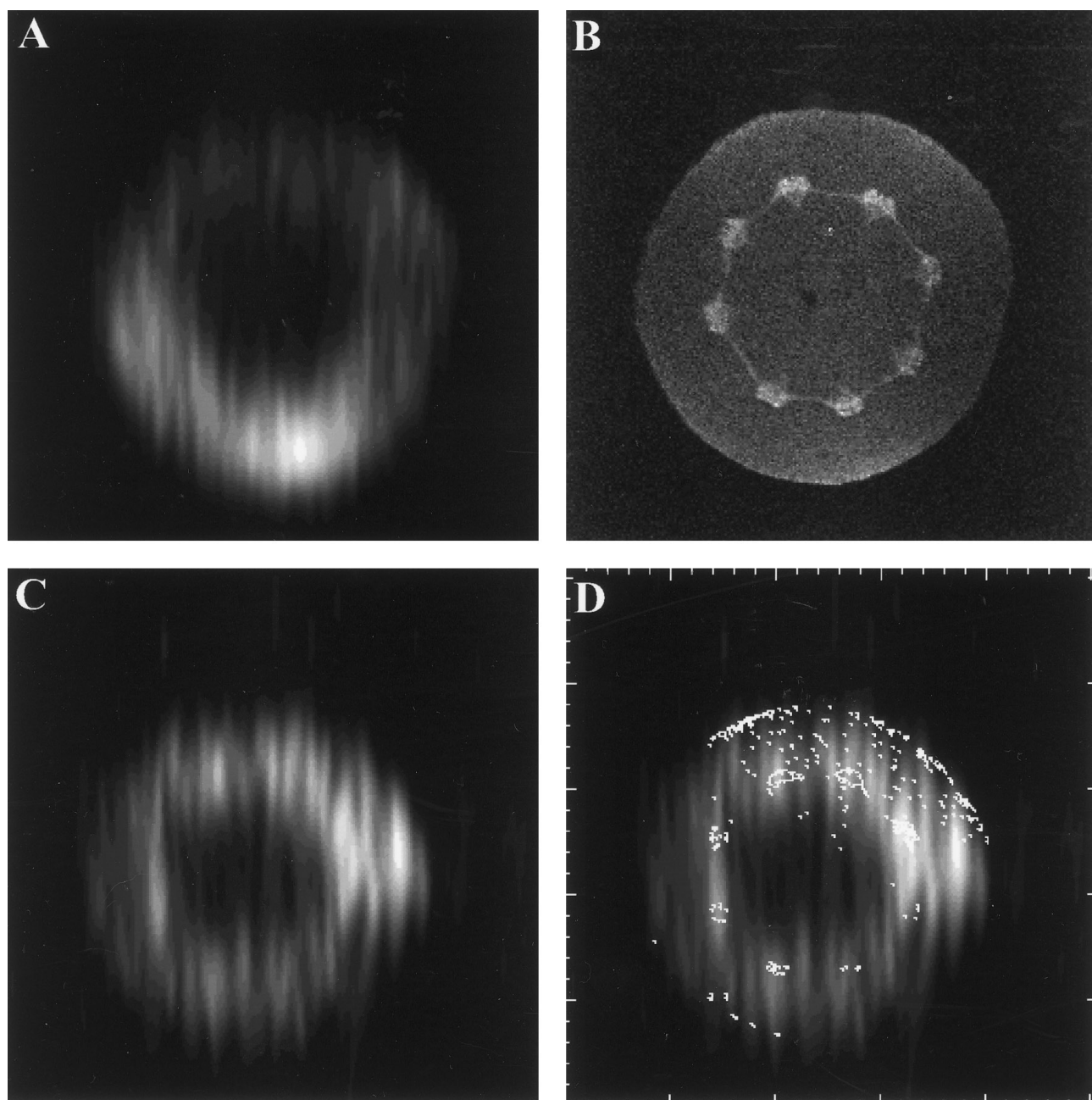
FIG. 12. *In vivo* indirect detected ^{13}C NMR images of the distribution of C1′-labeled sucrose within the hypocotyl of two different castor bean seedlings (A and C). C1′-labeled sucrose has been synthesized by the seedling after incorporation of labeled hexoses, ^{13}C$_1$ fructose and ^{13}C$_1$ glucose for 8 h. Acquisition and processing parameters of the edited images were 128 × 16 complex data points, T_E = 4 ms, number of scans = 600, T_R = 600 ms. A centered Hanning filter was applied prior to zero filling to 128 × 128 complex points and 2D Fourier transformation. The resolution of the edited images is 55 μm × 438 μm within the transverse plane. For reference, high resolution T_1-weighed spin echo proton image of the hypocotyl cross section is shown in (B). The matrix size of 256 × 256 complex points results in a resolution of 27 μm within the 1-mm slice. T_E was set to 8 ms and T_R = 300 ms. The pith parenchyma is inside the ring of meristematic tissue which connects the eight vascular bundles. The cortex parenchyma is outside this ring. Each vascular bundle consists of xylem and phloem. In (D), the CYCLCROP image of (C) is overlaid on the corresponding contour plot of a high resolution proton image.

mesophyll cells in the cotyledons, converted to sucrose, and then loaded into the phloem. Geigenberger *et al.* (*26*) measured the levels of a range of metabolites in the phloem sap after supplying fructose to the cotyledons. They observed a decreased concentration of UDP in the phloem sap and an increased concentration of inorganic phosphate. In their model, fructose is preferentially taken up in the phloem tissue and partially isomerized to glucose which subsequently

is metabolized to UDP-glucose. An equal incorporation of ^{13}C into the fructose moiety and the glucose moiety of the sucrose molecule would be expected from both models. However, the use of labeled compounds and *in vivo* NMR measurements has revealed a time-dependent use of the two hexoses in sucrose metabolism. This must be investigated by further NMR experiments.

Sucrose is loaded into the sieve tubes of the phloem and is transported through the hypocotyl toward the root system. Unloading occurs along the phloem pathway, but is higher in the upper part of the hypocotyl where a metabolic conversion to starch occurs. It is highest at the site where cells increase their volume by the uptake of water. This water uptake is osmotically driven, and sucrose possibly plays a role as an osmoticum which is either delivered by the phloem or synthesized from starch storages. The enrichment of labeled sucrose was monitored in our experiment at this site. The steady-state increase in signal intensity of the protons bound to either the ^{13}C nucleus of the fructose moiety or the glucose moiety clearly demonstrates transport and unloading of the labeled sucrose in this area. Different rates of increasing signal intensities arising from the three different slice positions are common to both the F1 and the G1 resonances of sucrose. This demonstrates that labeled sucrose is unloaded in the upper part of the hypocotyl and therefore concentration in the phloem sieve tubes decreases toward the root. Another explanation is a differential expression of the sucrose transporter along the phloem pathway. The decrease of concentration of labeled sucrose along the stem can also be seen in the edited profile of the F1 resonance of sucrose shown in Fig. 9.

Spin density maps of labeled sucrose in the hypocotyl revealed that sucrose, which was delivered by the phloem, either enters mainly the outer parenchymatic tissue, the cortex parenchyma, or is more rapidly metabolized in the pith parenchyma. Within the pith parenchyma, sucrose could be metabolized to the free hexoses glucose and fructose by the enzyme invertase. This would agree with the finding of correlation peak imaging experiments (*10*), where glucose was found mainly in the pith and sucrose mainly in the vascular bundles and the cortex parenchyma.

CONCLUSION

In our experiments, we used cyclic cross polarization under *in vivo* conditions for the first time in order to measure metabolic activity and transport of sucrose within intact castor bean seedlings. The technique used in the present study allowed an unambiguous identification of the labeled sucrose which is the product of the condensation of the supplied ^{13}C labeled hexoses, fructose and glucose. Since the F1 resonance of sucrose could be monitored by rapid acquisition of ^{13}C-edited proton spectra, the enrichment and transport in the hypocotyl of the seedling could be followed in a time course study. Spin density maps of the distribution of the

labeled sucrose within the plant stem could be obtained in a short measuring time. We conclude from our analysis of relaxational influences on the CYCLCROP signal that contrast in these maps is mainly created by differences in the concentration of the ^{13}C nuclei. The relatively short acquisition times of these images makes it feasible to map dynamical processes within the plant tissue with a reasonable time resolution on the order of less than one hour. The use of ^{13}C-labeled tracers in combination with indirect detection methods therefore promises to become a versatile tool in metabolic studies of living systems in general.

ACKNOWLEDGMENTS

REFERENCES

1. C. F. Jenner, Y. Xia, C. D. Eccles, and P. T. Callaghan, Circulation of water within wheat grain revealed by nuclear magnetic resonance imaging, *Nature* **336,** 339 (1988).

2. E. Kuchenbrod, M. Landeck, F. Thürmer, A. Haase, U. Zimmermann, Measurement of water flow in the xylem vessels of intact maize plants using flow-sensitive NMR imaging, *Bot. Acta* **109,** 184 (1996).

3. W. Köckenberger, J. P. Pope, Y. Xia, K. R. Jeffrey, E. Komor, P. T. Callaghan, A non-invasive measurement of phloem and xylem water flow in castor bean seedlings by nuclear magnetic resonance, *Planta* **201,** 53 (1997).

4. A. Metzler, W. Köckenberger, M. von Kienlin, E. Komor, A. Haase, Quantitative measurement of sucrose distribution in *Ricinus communis* seedlings by chemical-shift microscopy, *J. Magn. Reson. B* **105,** 249 (1994).

5. T. Y. Tse, R. M. Spanswick, L. W. Jelinski, Quantitative evaluation of NMR and MRI methods to measure sucrose concentrations in plants, *Protoplasma* **194,** 54 (1996).

6. C. Kunze, R. Kimmich, D. E. Demco, Cyclic and slice-selective *J* cross polarization for heteronuclear editing and localized NMR, *J. Magn. Reson. A* **101,** 277 (1993).

7. C. Kunze and R. Kimmich, Motion-insensitive localized ^{13}C spectroscopy using cyclic and slice-selective *J* cross polarization, *J. Magn. Reson. B* **105,** 38 (1994).

8. C. Kunze and R. Kimmich, Proton-detected ^{13}C imaging using cyclic *J* cross polarization, *Magn. Reson. Imaging* **12,** 805 (1994).

9. E. Komor, G. Orlich, J. Köhler, J. L. Hall, L. E. Williams, *in* ''Recent Advances in Phloem Transport and Assimilate Compartmentation'' (J. L. Bonnemain, S. Delrot, W. J. Lucas, J. Dainty, Eds.), p. 301, Ouest Editions, Nantes (1991).

10. A. Ziegler, A. Metzler, W. Köckenberger, M. Izquierdo, E. Komor, A. Haase, M. Décorps, and M. von Kienlin, Correlation peak imaging, *J. Magn. Reson. B* **112,** 141 (1996).

11. A. Morris and R. Freeman, Enhancement of nuclear magnetic resonance signals by polarization transfer, *J. Am. Chem. Soc.* **101,** 760 (1979).

12. S. R. Hartmann and E. L. Hahn, Nuclear double resonance in the rotating frame, *Phys. Rev.* **128,** 2042 (1962).

13. M. H. Levitt, D. Suter, R. R. Ernst, Spin dynamics and thermody-

namics in solid-state NMR cross polarization, *J. Chem. Phys.* **84**(8), 4243 (1986).

14. M. H. Levitt, Heteronuclear cross polarization in liquid-state nuclear magnetic resonance: Mismatch compensation and relaxation behaviour, *J. Chem. Phys.* **94**(1), 30 (1991).

15. R. Kimmich, ''NMR—Tomography, Diffusometry, Relaxometry,'' Springer-Verlag, Berlin (1997).

16. D. E. Demco, H. Köstler, R. Kimmich, Adiabatic *J* cross polarization with and without localization, *J. Magn. Reson. A* **110,** 136 (1994).

17. L. Müller and R. R. Ernst, Coherence transfer in the rotating frame. Application to heteronuclear cross-correlation spectroscopy, *Mol. Phys.* **38,** 963 (1979).

18. G. C. Chingas, A. N. Garroway, R. D. Bertrand, and W. B. Moniz, Zero quantum NMR in the rotating frame: *J* cross polarization in AX_N systems, *J. Chem. Phys.* **74,** 963 (1981).

19. N. Chandrakumar, G. V. Visalakshi, D. Ramaswamy, S. Subramanian, Analysis of collective modes in some $A_M X_N$ systems, *J. Magn. Reson.* **67,** 307 (1986).

20. O. W. Sørensen, A universal bound on spin dynamics, *J. Magn. Reson.* **86,** 435 (1990).

21. O. W. Sørensen, The entropy bound as a limiting case of the universal bound on spin dynamics. Polarization transfer in $I_N S_M$ spin systems, *J. Magn. Reson.* **93,** 648 (1991).

22. R. R. Ernst, G. Bodenhausen, A. Wokaun, ''Principles of Nuclear Magnetic Resonance in One and Two Dimensions,'' Oxford Univ. Press, London (1970).

23. D. C. McCain, The solution conformation of sucrose: Concentration and temperature dependence, *Carbohydr. Res.* **152,** 73 (1986).

24. P. T. Callaghan, ''Principles of Nuclear Magnetic Resonance Imaging,'' Oxford Univ. Press, Oxford (1991).

25. J. Kallarackal and E. Komor, Transport of hexoses by the phloem of *Ricinus communis L.* seedlings, *Planta* **177,** 336 (1989).

26. P. Geigenberger, S. Langenberger, I. Wilke, D. Heineke, D. W. Heldt, M. Stitt, Sucrose is metabolized by sucrose synthase and glycolysis within the phloem complex of *Ricinus communis L.* seedlings, *Planta* **190,** 446 (1993).